Supporting Information

A New High Resolution Ion Mobility Mass Spectrometer Capable of Measurements of Collision Cross Sections from 150-520K

Jakub Ujma,[a] Kevin Giles,[b] Michael Morris,[b] Perdita E. Barran.*[a]

[a] *Michael Barber Centre for Collaborative Mass Spectrometry, Manchester Institute for Biotechnology, University of Manchester, UK*

[b] *Waters, Wilmslow, UK*

1. Fundamental aspects of ion mobility measurements using linear field drift tube apparatus.

When placed inside the drift tube, ions experience a force imposed by the electric field and collisions with neutral gas molecules. If the applied field intensity ($E=U/L$) is sufficiently low and the gas number density (N) sufficiently high, ions will move with a constant velocity called a drift velocity ($v_d=L/t_d$). This velocity is proportional to the electric field intensity, with the ion mobility (K) being defined as the proportionality constant between v_d and E:

$$v_d = KE \qquad \text{or} \qquad t_d = \frac{L^2}{KU} \tag{1}$$

Thus ion mobility is a joint property of a particular ion and gas system and it can be seen as a measure of transparency of the gas medium to a given ion. This relationship is generally applicable to the cases where the ratio of E/N is sufficiently low, i.e. where ions' v_d is proportional to the E/N ratio and does not depend on E or N separately. This condition is a so called *low field limit* (LFL) and has been approximated by Mason and Revercomb[1] as:

$$\frac{E}{N} \ll \frac{3\pi d^2 k_B T}{q}\left(\frac{m}{m+M}\right)^{1/2} \tag{2}$$

Where q – charge, k_B – Boltzmann constant, T – gas temperature, d - sum of ion and neutral radii, m – mass of the molecule, M – mass of the neutral. Often expressed in units of Townsend (Td = 10^{-17} Vcm^2), E/N limit for singly charged atomic ions is about 6 Td. For larger ions the LFL is expected to be higher. Below the low field limit, ion mobility is inversely proportional to the ion-molecule interaction, which can be approximated by either a simple hard sphere collision cross section ($\sigma = \pi d^2$) or a diffusion collision cross section $\Omega_d(T_{eff})$ – a fundamental quantity of a *two temperature kinetic theory*.[2] Throughout this report we

refer to the latter quantity as collision cross section (CCS). A so called *fundamental ion mobility relation*[1–5] - the expression relating ion mobility to the CCS is presented below:

$$K \approx \frac{3}{16}\frac{q}{N}\left(\frac{1}{M}+\frac{1}{m}\right)^{1/2}\left(\frac{2\pi}{k_B T_{eff}}\right)^{1/2}\frac{1}{\Omega_D(T_{eff})} \quad (3)$$

Where the effective ion temperature (T_{eff}) is defined as:

$$T_{eff} = T + \frac{M(KE)^2}{3k_B} \quad (4)$$

The ion mobility is usually reported in terms of reduced mobility K_0, after normalisation to standard pressure and temperature:

$$K_0 = K\frac{P}{760}\frac{273.15}{T} \quad (5)$$

In the linear field, drift tube ion mobility measurements, we determine the drift times (t_d) – the time ions require to traverse through the drift cell. Particularly in the case of using MS detection, measured time ($t_{measured}$) inevitably contains a so called "dead time" – which correspond to the time ions spend between the end of the drift region and the detector ($t_{measured} = t_d + t_{dead}$). We combine and rearrange equations 1 and 5, including the effect of the dead time:

$$t_{measured} = \frac{1}{K_0}\frac{P}{U}\frac{L^2 273.15}{T\ 760} + t_{dead} \quad (6)$$

Having the times measured across the range of the pressure to voltage ratios (*P/U*), we can determine the reduced mobility from the resulting linear relationship where the slope equals to $1/K_0$ and the dead time corresponds to the intercept. With the knowledge of the dead time, one can combine equations 3, 5 and 6 to convert the measured drift time to CCS.

Detailed mathematical analysis of the ionic motion inside the linear field drift tube has been performed by Moseley *et al*.:[4,6,7]

$$\Phi(0,x,t) = \frac{sae^{-\alpha t}}{2}\left(v_d + \frac{L}{t_d}\right) \times \left[1 - \exp\left(-\frac{{r_0}^2}{4D_y t}\right)\right]\frac{\exp\left(-\frac{(L-v_d t)^2}{4D_x t}\right)}{\sqrt{4\pi D_x t}} \quad (7)$$

The above equation calculates the flux of ions passing through the exit aperture of the DT-IMS device as a function of drift time t_d and drift distance L along the direction x. Ion packet of a density s is starting the drift from the infinitely thin disc of the diameter r_0 and are detected on a detector of the area a placed at

the distance *L*. The rate of loss of ions via reactions with the drift gas is accounted for via the parameter *α*. In summary, the first term in the equation concerns the source and detector conditions, second term relates to diffusion driven transverse spread of ion packet and the last term describes the diffusion driven spread of the ion packet along the drift axis *x*. If the device is operating under the low field conditions, transverse and longitudinal diffusion coefficients will be equal ($D_y = D_x$) and are related to mobility through the Nernst-Einstein-Townsend relation:

$$D = \frac{k_B T}{q} K \tag{8}$$

The above equation can be used to calculate the theoretical arrival time distributions (ATD) and in particular predict the width of the ATD, expected for the ion of a particular mobility or CCS. Moreover, it is possible to utilise it to derive the theoretical maximum of the resolving power of the IMS device, limited by diffusion. Resulting quantity is a so called diffusion limited resolving power (R_{max}):

$$R_{max} = \frac{t_{drift}}{\Delta t} = \sqrt{\frac{d\ q\ E}{16\ k_B T \ln 2}} \tag{9}$$

Where t_{drift} corresponds to the maximum of ATD, and Δt to full width at half maximum (FWHM) of the ATD peak. An exact match of R_{exp} and R_{max} is rarely achieved in the experimental reality. This is primarily because initial pulse of ions is not infinitively thin; ions rarely exist in a single conformation, ions require some focussing and transmission through regions of different pressure which can cause longitudinal spread of the pulse and finally detection, digitisation and data acquisition can all have negative effect on the measured resolving power. Conditional resolving power equations based on more realistic theoretical[8–10] and empirical[11,12] models have been proposed. Notably, a characteristic relatively straight forward to implement is the initial pulse width (Δt_{gate}).[8,9] The conditional resolving power relation including the effect of the initial gate time is:

$$R_{cond} = \frac{t_{drift}}{\Delta t} \approx t_{drift} \left({\Delta t_{gate}}^2 + \frac{{t_{drift}}^2}{{R_{max}}^2} \right)^{-1/2} \tag{10}$$

Nevertheless, by comparing the experimentally determined resolution to the R_{max}, one can assess the overall instrument performance. In view of previous work in the field,[13–17] for a home built, low pressure, ambient IM-MS configuration R_{exp}/R_{max} around 0.7- 0.95 can be anticipated. According to the equation 9, the resolving power should have an inverse square root dependence on the temperature; however a scarce amount of work has been done to investigate this effect experimentally. May and Russell have reported an increase in the R_{max} at reduced temperatures, however not to the theoretically predicted extent.[16]

Finally, we ought to mention some of the limitations of the currently used theory. It was primarily developed to model the changes in mobility with varying field strength for small, singly charged, atomic ions such as alkali metals.[2] Despite its success describing such systems,[18,19] its applicability to

describe interactions of gas with the large, multiply charge ions may be limited and certainly requires further theoretical and experimental investigations. We note that recently Siems, Viehland and Hill have expressed concerns regarding the approximations used to define the low field limit condition and propose new definition based on relative velocities of ion and gas molecules.[5] Another important consideration is that the current theory only holds in a so called molecular ion regime; that is where collisions between ion and gas are binary. When multiple collisions occur simultaneously, ion movement becomes dependent on gas viscosity, ultimately leading to "Stokes like" flow scenario.[4] This effect becomes significant when the mean free path of the gas molecule (λ) becomes comparable to the diameter of the ion. Milikan has investigated this phenomenon experimentally during his famous oil drop experiment.[20,21] Subsequent analysis was performed by Annis and Malinauskas.[22] From their data it is possible to estimate that at standard conditions, some effects of the viscous flow could be anticipated for ions with $\sigma > 10^4$ Å². At low pressures used in our instrument this effect scales favourably by several orders of magnitude. However, this estimate is based on hard-sphere like interaction with the neglect of long range attractive interactions.

2. Further Details on Mechanical and Electronic Design

Chamber Design and Temperature Control

The ion source chamber is attached to the ion mobility assembly *via* a 3 cm thick ceramic break (99.8% Al_2O_3, Multi-Lab, UK), compressed between the two stainless steel flanges using four M8 bolts in insulating PEEK sleeves. The seal between the metal and ceramic is achieved *via* spring energized seals. The sealing interface is of a flat face design, thus allowing for differential radial expansion of the ceramic break and the stainless steel flanges. One of the stainless steel flanges is interfaced with the source chamber *via* a spring energized seal, while the other is connected to the external IMS chamber *via* a knife edge/copper gasket (CF160). A similar insulating interface is used on the other end side of the IMS assembly. The conical aperture at the end of the drift region is sealed to the ceramic flange using a spring energized, filled PTFE seal. Compression is achieved through a molybdenum ring (The Mists of Avalon, Ebay), attached to the ceramic flange with three M3 molybdenum screws. Molybdenum and alumina have similar thermal expansion coefficients, therefore risk of thermal misalignment and breaking of the ceramic flange during thermal cycling is minimised. The external IMS chamber features a flexible bellow and three CF40 ports. One of these is used for mechanical pump connection, one for 2x thermocouple (Type K, Allectra UK) and 2x heater power supply (8 amp, Allectra UK) and the remaining one for 2x LN2 feedthrough (2x Swagelok 1/4", Kurt Lesker, UK).

We noted that during VT experiments, the temperature of the ceramic breaks is different from the temperature of the electrode assembly. However, the temperature the ions experience throughout the drift region should be constant and close to that measured with the Pt100 thermometers. The reasons for this are as follows: i) the majority of the thermal transfer occurs through the supporting ceramic rings and thick rods; ii) the beginning of the drift region is about 8 cm away from the source ceramic break; iii) the end of the ion funnel is about 2 cm away from the corresponding ceramic break; iv) the temperature is

measured very near the drift electrodes; v) the overall length of the drift region is significantly longer than the interface regions where temperature gradients are expected. Typically, during VT-CCS measurements, the temperature difference between two ends of the drift region is <5K which corresponds to an error in determined $^{DT}CCS_{He}$ values of <2%. In this work we present data obtained at temperatures down to 150K. Cooling to lower T (100K) is possible, but requires precooling of the drift gas to reduce this temperature discrepancy. Typically, during prolonged heating to 500K, the temperature of the external parts of the IMS chamber does not exceed 320K. Likewise, during prolonged cooling, the temperature of the external chamber does not fall below 280K. During humid weather, this can cause a small amount of condensation; however it is easily alleviated by inducing air circulation around the chamber with a fan.

Internal Electronic Components

The electronic components used inside the ion mobility drift tube have been carefully chosen based on temperature ratings and low outgassing characteristics. We have used high temperature resistors (Power Film Resistors, 1 MΩ, rated up to 550K, Caddock, USA) and high temperature capacitors (Multilayer Ceramic Capacitors, 1000 pF, rated up to 500K, Kemet, USA). Resistors are attached to drift rings using cable lugs (nickel plate copper, Allectra UK) and M2 bolts. Gold plated pins (BeCu, VB series, VACOM, Germany) are attached to the ion funnel and buncher electrodes. Printed circuit boards were manufactured from filled PTFE material (rated up to 580K, Rogers 3003, Rogers, USA). PCBs containing capacitors, resistors and gold plated beryllium copper sockets slot onto the electrodes of the ion funnel and buncher. One board is used for each RF phase. Resistors, capacitors and pins were soldered on to the PCBs using UHV compatible, high temperature solder (Pb/Ag, melting point 575 K, Allectra, UK). The electrical schematic of the ion buncher and the ion funnel resemble those reported by Shaffer *et al.*.[22] The modified miniature feedthroughs and sockets (10 and 12 pin, VB series, VACOM, Germany) have been compressed on both ceramic flanges to provide all necessary electrical connections. Kapton insulated copper wire (38 AWG, Allectra, UK) has been used throughout. All of the above components were bench tested while repeated immersing in liquid nitrogen and heating up to ~600K using a propane torch.

Modifications to Instrument Acquisition/Control System

The data acquisition and instrument control system have been updated. The original motherboard in the embedded PC has been replaced with the motherboard from a QToF Premier instrument (Waters). This was done in order to incorporate a newer generation time to digital converter (TDC) card (4GHz, TTP Instruments, UK) and to increase the amount of RAM memory available for IMS acquisition over extended mass ranges. The operating system (VxWorks, Waters) of the embedded computer was also updated in order to enable IMS-ToF acquisition. The IMS enabled development version of MassLynx software from the early 2000s[26,44] has been used in this work. Application settings have been modified further in order to allow IMS acquisition of quadrupole selected ions using the built in photomultiplier.

Electronics

Voltage pulses are provided to the ion buncher grids using a pulse amplification circuit adapted from the work of Kemper and Bowers (private communication). Due to the relatively low capacitance of our RF devices we can adapt hexapole driver boards from Waters instruments.

We have designed and built a main DC power supply consisting of 12 electrically floatable modules which can be connected in series or in parallel depending on the needs. Schematic of such module is presented in the figure S2. Briefly, 15VDC generated by the AC/DC converter is provided to an isolating DC/DC converter (RE1, 4 kV isolation, RECOM). Isolated 15VDC from DC/DC converter is supplied to voltage regulator (LM317, Fairchild). Knob of the potentiometer (Pot_1) is electrically insulated from the PSU chassis via long plastic rod. Using Pot_1 we can regulate the output of RE1 between 2 and 12VDC. Regulated DC is supplied into proportional DC/DC converter (Q1, Q-Series, EMCO, USA), which converts 2-12VDC input into 10-700VDC output (0.7 mA). This output is connected to the appropriate electrode via 5MOhm resistor and directly connected to a consecutive board to provide the reference voltage. Voltage divider (R2, R3) divides the output from EMCO converter by 1000. Scaled output is fed into isolation amplifier (AD1, AD202KY, Analog Devices, USA, 2kV isolated ±5VDC output). Isolated monitor voltage is connected into Adruino board, scaled and displayed on the LCD screen. Relays (S1, S2, 4 kV isolation, 1kV switching, SIL series, MEDER, USA), are used to switch the input reference and output bias voltages for positive and negative polarities. High voltage connectors (5kV, BA series, FcLane, UK) were used for the output; 5kV rated cable has been used throughout. Each module manufactured as separate PCB featuring high and low voltage sides. This relatively simple design enabled us to connect the boards in many different configurations and is safely floatable into 2kV region (4kV if we opted out from AD202KY voltage monitor).

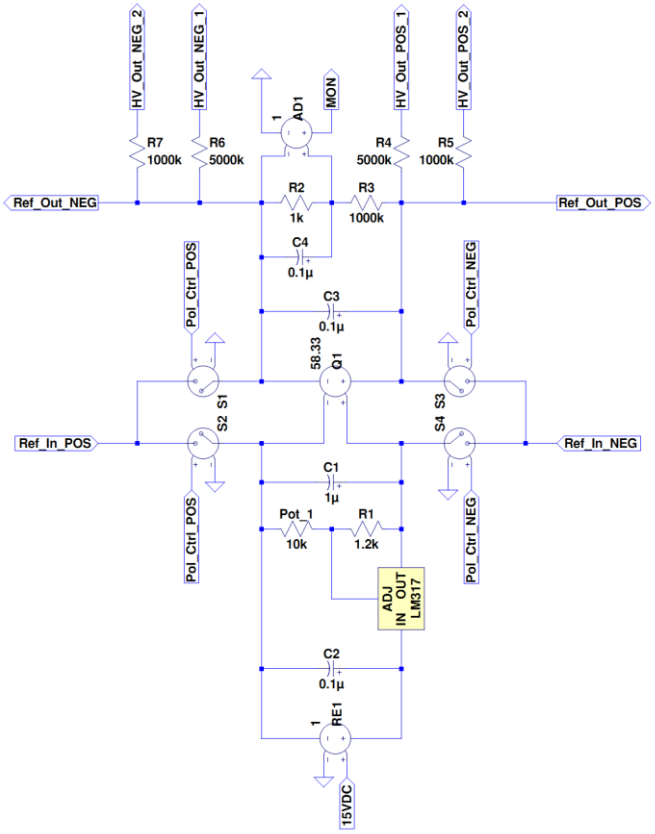

Figure S2. Electrical Schematic of a floatable DC module.

References

[1] Revercomb, H. E.; Mason, E. A. *Anal. Chem.* **1975**, *47* (7), 970–983

[2] Viehland, L. A.; Mason, E. A. *Ann. Phys. (N. Y).* **1978**, *110* (2), 287–328

[3] Langevin, M. P. *Ann. Chim. Phys.* **1905**, *8*, 245–277.

[4] Mason, E. A.; McDaniel, E. *Transport Properties of Ions in Gases*; 1988.

[5] Siems, W. F.; Viehland, L. A.; Hill, H. H. *Anal. Chem.* **2012**, *84*, 9782–9791.

[6] Moseley, J. T.; Snuggs, R. M.; Martin, D. W.; McDaniel, E. W. *Phys. Rev.* **1969**, *178* (1), 240–248

[7] Moseley, J. T.; Gatland, I. R.; Martin, D. W.; McDaniel, E. W. *Phys. Rev.* **1969**, *178* (1), 234–239.

[8] Kanu, A. B.; Gribb, M. M.; Hill, H. H. *Anal. Chem.* **2008**, *80* (17), 6610–6619

[9] Rokushika, S.; Hatano, H.; Bairn, M. A.; Hill, H. H. *Anal. Chem.* **1985**, *57*, 1902–1907.

[10] Verbeck, G. F.; Ruotolo, B. T.; Gillig, K. J.; Russell, D. H. *J. Am. Soc. Mass Spectrom.* **2004**, *15* (9), 1320–1324

[11] May, J. C.; Dodds, J. N.; Kurulugama, R. T.; Stafford, G. C.; Fjeldsted, J. C.; McLean, J. A. *Analyst* **2015**, *140* (20), 6824–6833

[12] Siems, W. F.; Wu, C.; Tarver, E. E.; Hill, H. H. J.; Larsen, P. R.; McMinn, D. G. *Anal. Chem.* **1994**, *66* (23), 4195–4201

[13] Tang, K.; Shvartsburg, A.; Lee, H.-N.; Prior, D. C.; Buschbach, A.; Li, F.; Tolmachev, A. V; Anderson, G. A.; Smith, R. D. *Anal. Chem.* **2005**, *77* (10), 3330–3339

[14] Kemper, P. R.; Dupuis, N. F.; Bowers, M. T. *Int. J. Mass Spectrom.* **2009**, *287* (1-3), 46–57

[15] Clowers, B. H.; Hill, H. H. *Anal. Chem.* **2005**, *77* (18), 5877–5885

[16] May, J. C.; Russell, D. H. *J. Am. Soc. Mass Spectrom.* **2011**, *22* (7), 1134–1145

[17] Ibrahim, Y. M.; Baker, E. S.; Danielson, W. F.; Norheim, R. V.; Prior, D. C.; Anderson, G. A.; Belov, M. E.; Smith, R. D. *Int. J. Mass Spectrom.* **2014**, *377*, 655–662

[18] Gatland, I. R.; Viehland, L. A.; Mason, E. A. *J. Chem. Phys.* **1977**, *66* (2), 537–541

[19] Viehland, L. A. *Chem. Phys.* **1983**, *85*, 291.305.

[20] Milikan, R. A. *Phys. Rev.* **1923**, *22*, 1–23.

[21] Millikan, R. A. *Phys. Rev. (Series I)* **1911**, *32* (4), 349–397

[22] Annis, B. K.; Malinauskas, A. P. *Aerosol Sci.* **1972**, *3* (1), 55–64.